(1914); English translation available in Brillouin, L. *Wave Propagation and Group Velocity* Ch. III (Academic, New York, 1960).
12. Chu, C. & Wong, S. Linear pulse propagation in an absorbing medium. *Phys. Rev. Lett.* **48,** 738–741 (1982).
13. Ségard, B. & Macke, B. Observation of negative velocity pulse propagation. *Phys. Lett.* **109,** 213–216 (1985).
14. Peatross, J., Glasgow, S. A. & Ware, M. Average energy flow of optical pulses in dispersive media. *Phys. Rev. Lett.* **84,** 2370–2373 (2000).
15. Wang, L. J., Kuzmich, A. & Dogariu, A. Gain-assisted superluminal light propagation. *Nature* **406,** 277–279 (2000).
16. Akulshin, A. M., Cimmino, A. & Opat, G. I. Negative group velocity of a light pulse in cesium vapor. *Quantum Electron.* **32,** 567–569 (2002).
17. Bigelow, M. S., Lepeshkin, N. N. & Boyd, R. W. Superluminal and slow light propagation in a room-temperature solid. *Science* **301,** 200–202 (2003).
18. Cao, H., Dogariu, A. & Wang, L. J. Negative group delay and pulse compression in superluminal pulse propagation. *IEEE J. Sel. Top. Quantum Electron.* **9,** 52–58 (2003).
19. Macke, B. & Ségard, B. Propagation of light-pulses at a negative group velocity. *Eur. Phys. J. D* **23,** 125–141 (2003).
20. Steinberg, A. M. & Chiao, R. Y. Dispersionless, highly superluminal propagation in a medium with a gain doublet. *Phys. Rev. A.* **49,** 2071–2075 (1994).
21. Harris, S. E. Electromagnetically induced transparency. *Phys. Today* **50,** 36–42 (1997).
22. Stenner, M. D. & Gauthier, D. J. Pump-beam-instability limits to Raman-gain-doublet "fast-light" pulse propagation. *Phys. Rev. A.* **67,** 063801 (2003).
23. Diener, G. Superluminal group velocities and information transfer. *Phys. Lett. A* **223,** 327–331 (1996).
24. Wynne, K. Causality and the nature of information. *Opt. Commun.* **209,** 85–100 (2002).
25. Mitchell, M. W. & Chiao, R. Y. Negative group delay and "fronts" in a causal system: An experiment with very low frequency bandpass filters. *Phys. Lett. A* **230,** 133–138 (1999).
26. Nakanishi, T., Sugiyama, K. & Kitano, K. Demonstration of negative group delays in a simple electronic circuit. *Am. J. Phys.* **70,** 1117–1121 (2002).
27. Solli, D., Chiao, R. Y. & Hickmann, J. M. Superluminal effects and negative group delays in electronics, and their applications. *Phys. Rev. E* **66,** 056601 (2002).
28. Kuzmich, A., Dogariu, A., Wang, L. J., Milonni, P. W. & Chiao, R. Y. Signal velocity, causality, and quantum noise in superluminal light pulse propagation. *Phys. Rev. Lett.* **86,** 3925–3929 (2001).
29. Caves, C. M. & Drummond, P. Quantum limits on bosonic communication rates. *Rev. Mod. Phys.* **66,** 481–537 (1994).

Acknowledgements M.D.S. and D.J.G. acknowledge discussions with M. Gehm and J. Thomas, the loan of an argon-ion pump laser from J. Thomas, and the financial support of the US National Science Foundation.

Competing interests statement The authors declare that they have no competing financial interests.

Correspondence and requests for materials should be addressed to D.J.G. (gauthier@phy.duke.edu).

Single-electron transistor of a single organic molecule with access to several redox states

Sergey Kubatkin[1], Andrey Danilov[1], Mattias Hjort[2], Jérôme Cornil[2,3], Jean-Luc Brédas[2,3]*, Nicolai Stuhr-Hansen[4], Per Hedegård[4] & Thomas Bjørnholm[4]

[1]*Department of Microtechnology and Nanoscience/MC2, University of Technology, Chalmers, Göteborg, Sweden*
[2]*Department of Chemistry, The University of Arizona, Tucson, Arizona 85721-0041, USA*
[3]*Laboratory for Chemistry of Novel Materials, Center for Research in Molecular Electronics and Photonics, University of Mons-Hainaut, Place du Parc 20, B-7000 Mons, Belgium*
[4]*Nano-Science Center (Department of Chemistry and Niels Bohr Institute), University of Copenhagen, Universitetsparken 5, DK-2100, Copenhagen, Denmark*

* Present address: School of Chemistry and Biochemistry, Georgia Institute of Technology, Atlanta, Georgia 30332-040, USA

A combination of classical Coulomb charging, electronic level spacings, spin, and vibrational modes determines the single-electron transfer reactions through nanoscale systems connected to external electrodes by tunnelling barriers[1]. Coulomb charging effects have been shown to dominate such transport in semiconductor quantum dots[2], metallic[3] and semiconducting[4] nanoparticles, carbon nanotubes[5,6], and single molecules[7–9]. Recently, transport has been shown to be also influenced by spin—through the Kondo effect—for both nanotubes[10] and single molecules[8,9], as well as by vibrational fine structure[7,11]. Here we describe a single-electron transistor where the electronic levels of a single π-conjugated molecule in several distinct charged states control the transport properties. The molecular electronic levels extracted from the single-electron-transistor measurements are strongly perturbed compared to those of the molecule in solution, leading to a very significant reduction of the gap between the highest occupied molecular orbital and the lowest unoccupied molecular orbital. We suggest, and verify by simple model calculations, that this surprising effect could be caused by image charges generated in the source and drain electrodes resulting in a strong localization of the charges on the molecule.

We measured electrical transport at 4 K through a single *p*-phenylenevinylene oligomer, which has five benzene rings connected through four double bonds (OPV5, Fig. 1a). OPV5 was placed by chemical vapour deposition in a gap about 2 nm wide separating the source and drain electrodes of a single-electron transistor (SET) device (Fig. 1). The synthesis of OPV5 ((*E*,*E*)-1,4-bis{4-{(E)-4-(*tert*-butylthio)styryl}}benzene) was done by a Horner–Wadsworth–Emmons condensation[12] of tetraethyl 1,4-xylylenediphosphonate with *trans*-4-(*tert*-butylthio)styrylbenzaldehyde. The terminal thiols were protected with a *tert*-butyl group, which prevents chemical binding of the sulphur to the gold electrode and leads to a weak van der Waals contact between the molecule and the source and drain electrodes.

A planar gate electrode made of aluminium metal covered with aluminium oxide (~5 nm thick) was prepared on a chip of oxidized silicon. A shadow mask used to deposit the gold lead electrodes was defined on top of the gate by standard electron-beam lithography. The chip was then introduced into a vacuum chamber immersed in liquid helium. All subsequent procedures reported here were performed during a single vacuum cycle. First, two gold electrodes were deposited through a shadow mask by condensing gold vapour on the substrate held at 4.2 K. By using an oblique evaporation angle (Fig. 1b) together with *in situ* conductance measurements, we were able to fine-tune the tunnelling gap between the gold electrodes to a few nanometres[13]. As shown in Fig. 1b, for an inclined beam, a constriction is formed by two mask edges. If the tilt angle is high, there is no overlap between source and drain shadows. Reducing the tilt angle decreases the source–drain gap. We changed the tilt stepwise, narrowing the gap between the leads by 5 nm at each step. At each step, a 2-nm-thick film of gold was deposited through the mask and the sample was checked for non-zero tunnelling conductance (this procedure of nanometre-scale gap fabrication has been successfully tested for other metals[13]). Eventually, we fabricated two self-aligned and self-sharpened gold electrodes with a tunnelling gap of a few MΩ between them. By annealing the sample up to 100 K, we increased the gap resistance to a few GΩ, which corresponds to a tunnelling gap width of roughly 2 nm (ref. 14). Annealed samples did not show any gate dependence of the tunnelling conductance nor any peculiarities in the current–voltage, $I(V)$, curves. In a separate control experiment, we observed that an irreversible decomposition of gold into separate clusters starts at 150–200 K.

Second, a submonolayer (~1%) of organic molecules was deposited on the electrodes by quench condensation. The sample was annealed at low temperature (below 70 K) allowing thermally activated motion of the organic molecules, while monitoring the nanogap conductance at a source–drain bias of 400 mV. When the conductance changed stepwise, indicating the trapping of a single molecule in the nanogap, the device was cooled to a temperature of 4.2 K where all transport measurements were taken. This entire process was repeated successfully for three independent devices.

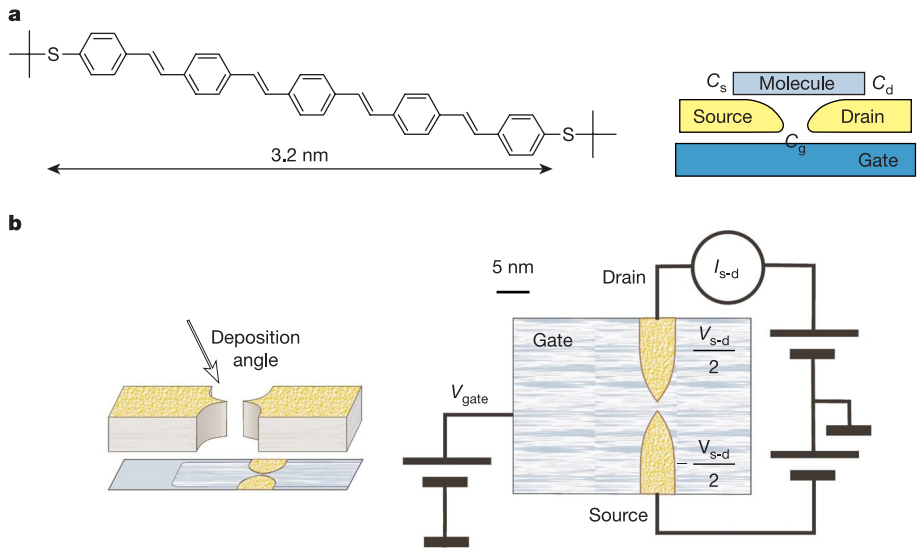

Figure 1 Device and experiment. **a**, Molecular structure of OPV5 and schematic experimental set-up. **b**, Schematic representation of the device preparation procedure.

By changing the gate voltage (V_g) of the SET with a single molecule in the nanogap in small steps from -4.3 V to $+4.3$ V while measuring the source–drain current–voltage characteristics ($I_{s\text{-}d}$–$V_{s\text{-}d}$) at each step (Fig. 2), we were able to probe eight different transmitting (open) states of the SET. This is summarized in Fig. 2a, where the differential conductance ($dI_{s\text{-}d}/dV_{s\text{-}d}$) of the SET is plotted in colour code as a function of the gate voltage (V_g) and source–drain voltage ($V_{s\text{-}d}$). The dark diamonds in Fig. 2a correspond to zero-current regions, where the low bias transport is blocked. Not all of the dark diamonds are complete, because the measurements were taken in a limited $V_{s\text{-}d}$ range of ± 75 mV (at higher source–drain voltages the sample was unstable, possibly owing to the switching between different molecular conformations).

Two features emerge from the data set: (1) all diamond edges (the lines separating transmitting and closed regions) are straight and possess only two characteristic slopes, one positive and one negative; and (2) contrary to cases where SETs are dominated by Coulomb charging alone, the zero-bias open states are distributed in a non-equidistant way along the V_g axis, implying that effects other than simple Coulomb charging dominate the properties of our device. Around $V_g \approx 0$ these states clearly appear in bunches of two.

The linearity of the diamond edges allows us to express the electrostatic interaction between the molecule and gate and lead electrodes in terms of three effective capacitances (C_s, C_d, C_g, Fig. 1a). This is known as the capacitance model[15,16]. We note that linear diamond edges have also been observed in other experiments with gated molecules[7,8]. The data in Fig. 2a show that the same set of capacitances characterizes the SET for all charged states of the molecule. This in turn proves that we are dealing with a system with just two tunnelling gaps—that is, with only one molecule connecting the source and drain electrodes—because a system with more than one quantum dot always has more than two characteristic slopes[17].

To further investigate the second feature of our data, we use the capacitance model introduced above to extract the energies required to add an extra charge to a particular molecular ion. According to the theory of SET operation[15,18], the molecule can pass charge through the SET at every open state of the transistor by switching between two states with charge $(n + 1)e$ and ne, where e denotes the electron charge (-1.6×10^{-19} C). The corresponding open state

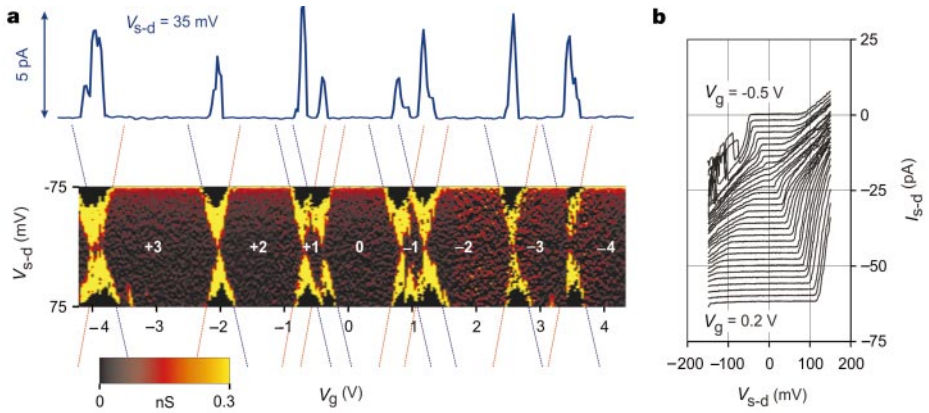

Figure 2 Experimental results. **a**, Measurements of the differential conductance ($dI_{s\text{-}d}/dV_{s\text{-}d}$) as function of $V_{s\text{-}d}$ and V_g. All red lines, and all blue lines, have identical slopes, as discussed in the text. The full solid line at the top of the figure shows a representative $I_{s\text{-}d}$–V_g trace. **b**, Examples of current–voltage curves $I_{s\text{-}d}$–($V_{s\text{-}d}$) for a single OPV5 molecule obtained at different gate potentials V_g (temperature $T = 4.2$ K). Curves are shifted vertically for clarity.

gate voltages $V_g(n)$ are defined by matching the electrochemical potentials of the electrodes and the OPV molecule: $\mu_{ELECTRODE} = \mu_{OPV}(n, V_g(n))$. The electrochemical potential $\mu_{OPV}(n, V_g)$ is the difference between the ground state energies E for the two differently charged ions at a gate voltage V_g : $\mu_{OPV}(n, V_g) = E(n, V_g) - E(n-1, V_g)$. According to the capacitance model, the gate voltage shifts the electrochemical potential of the molecule linearly, allowing us to relate the diamond sizes along the gate axis to the molecular charging (electron addition) energies, $I(n \rightarrow n+1)$, by:

$$I(n \rightarrow n+1) = \mu_{OPV}(n+1,0) - \mu_{OPV}(n,0)$$

$$= (C_g/(C_s + C_d + C_g))e(V_g(n) - V_g(n+1)) \quad (1)$$

where the scaling factor $C_g/(C_s + C_d + C_g)$ equals the ratio of the Coulomb diamond size along bias and gate axes multiplied by 2 as also shown in ref. 16 for a metallic island. We can use any of the two complete dark diamonds in Fig. 2a to estimate $C_g/(C_s + C_d + C_g)$, which turns out to be ~0.2.

In terms of atomic energies the addition energy is the difference between the ionization energy and the electron affinity[18]. For a quantum dot treated within a single-particle picture, the addition energy I equals the energy difference between two adjacent states plus the Coulomb energy $e^2/(C_s + C_d + C_g)$ (ref. 18). For the neutral molecule, this can be expressed as:

$$I(0 \rightarrow 1) = \varepsilon^{LUMO} - \varepsilon^{HOMO} + e^2/(C_s + C_d + C_g) \quad (2)$$

where $\varepsilon^{LUMO} - \varepsilon^{HOMO}$ is the single-particle gap between the highest occupied molecular orbital (HOMO) and the lowest unoccupied molecular orbital (LUMO).

From Fig. 2 and the addition energies listed in Table 1, it is clear that the addition or removal of an electron from the molecule in a particular electronic configuration is not reduced to a simple change of electrostatic energy in the system, but also involves the energy related to the occupation of quantum-mechanical states. In metallic islands or nanotubes, such effects are small owing to their high density of states[19]. For a molecule, we deal with the opposite situation where the discretization of electronic levels should dominate.

The data in Fig. 2a and Table 1 clearly reveal a symmetric bunching effect around $V_g = 0$, allowing us to use a symmetry argument for assigning this region to the neutral molecule. On the basis of this assignment, we have tabulated the charge on the molecule (redox state) in Table 1, together with independent molecular addition energies provided by the SET for both positively and negatively charged molecules. For comparison, we also list addition energies obtained from electrochemistry[20] and quantum-chemical calculations (Methods) for the negatively and positively charged redox states, respectively. The electrochemical and computational values have been scaled by the factors given in Table 1 to best match the trends in the SET data. Furthermore, the addition energy

Table 1 **Addition energies and redox states**

Redox state	n	$V_g(n)$ (V)	$I(n \rightarrow n+1)^{SET}$ (meV)			$I(n \rightarrow n+1)^{other}$ (meV)	
−4	4	3.53*	†	‡	*		
−3	3	2.64			162	60§	
−2	2	1.20			262	280§	
−1	1	0.84		60	66	70§	66#
0	0	−0.42		312	230	2,500 ‖	230#
1	−1	−0.77	70	56	63	39¶	66#
2	−2	−2.13	390	266	247	350¶	
3	−3	−4.10			358	165¶	

Symbols are defined in the text.
*Data in these two columns are from Fig. 2a, representing the essence of many measurements on the same device/molecule.
††Data in these two columns are from two additional devices prepared independently. The ratio $C_g/(C_s + C_d + C_g) = 0.2$.
§From electrochemical midway potentials (ref. 20) multiplied by a scaling factor of 0.5.
‖Estimated from absorption edge of OPV5 in solution situated at 450 nm (own data).
¶Estimated from computed ionization potentials (AM1, dielectric constant = 2.5, as suggested from data in ref. 25) multiplied by a scaling factor of 0.16.
#Addition energies calculated by a Hubbard model (see Methods) representing the molecule as 38 p_z carbon orbitals with an on-site repulsion U and a transfer integral t between connected atoms. Image charges have been included by changing the on-site energy on one or both terminal benzene ring(s) by an amount equal to the mirror image charge energy, Φ, given by $\Phi_{image} = 27.2$ (eV Å)/(ε_r a), where ε_r is the relative dielectric constant and a the distance between the charge and its image in ångströms. The values listed in Table 1 are obtained by fitting t to the optical HOMO–LUMO gap of the pristine OPV5 molecule (2,500 meV). The two independent parameters (ε_r a) and U are obtained by fitting the model to the experimental addition energies obtained for $n = -1, 0, +1$. The resulting values are: $t = 3.92$ eV, $U = 4.27$ eV, (ε_r a) = 4.7 Å. The value of (ε_r a) is in good agreement with the expected distance between the plane of the benzene ring and its image when the benzene ring is in van der Waals contact with the electrode. The charges are thus expected to be separated by roughly twice the van der Waals radius of sp^2-hybridized carbon (~3 Å). U is also well within the expected range for on-site repulsion in organic molecules.

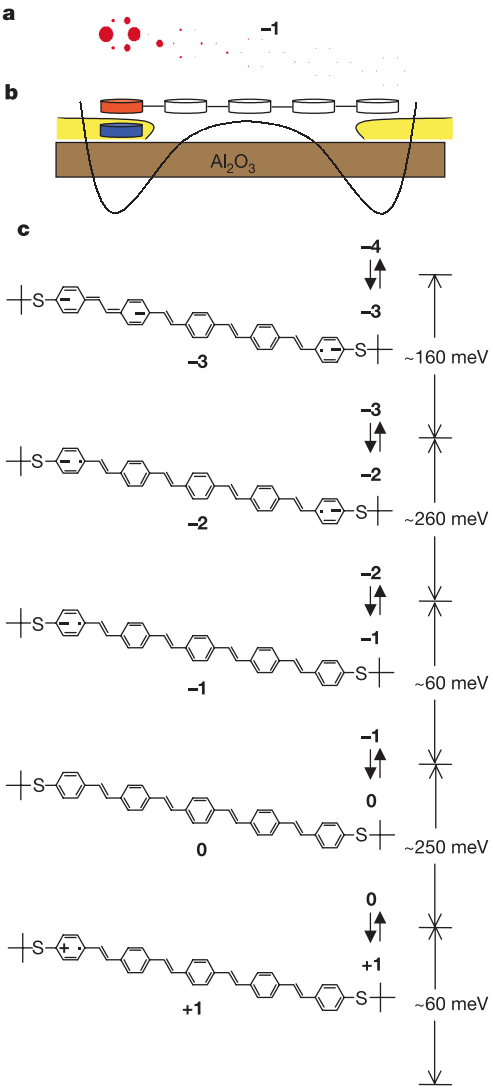

Figure 3 Calculations of charge confined on the OPV5 molecule, and valence bond models of the redox states involved. **a**, Charge distribution calculated by a Hubbard model for a single charge trapped on the OPV5 molecule and stabilized by its image charge; the size of the red circles is proportional to the atomic charge density. **b**, Schematic representation of the effective potential of a charge confined on the OPV5 molecule and influenced by its image charges in the source and drain electrodes (full line). The blue and red-coloured rings illustrate the equilibrium position of the image charge in the electrode and the charge on the molecule, respectively. **c**, Selected valence bond models of the involved redox states (left side) and corresponding addition energies (right side) between open states involving the redox couples indicated by the double arrows.

for the neutral molecule ($\sim\varepsilon^{\mathrm{LUMO}} - \varepsilon^{\mathrm{HOMO}}$), which is not directly available from electrochemical measurements, has been estimated from the onset of the absorption spectrum of OPV5.

The comparison between SET addition energies and the electrochemical and computational values shows similar evolutions for both the positive and negative redox states. But for the neutral molecule, there occur marked deviations among the data; the spectroscopic HOMO–LUMO gap (~2.5 eV) is one order of magnitude larger than the HOMO–LUMO gap extracted from the SET data, according to equation (2) (~0.2 eV). The rather large scaling factors required to match the electrochemical and computational values to the SET data and the dramatic change in the HOMO–LUMO gap strongly indicate that the intrinsic electronic level spacings of the molecule have been significantly altered in the metallic junction. On the basis of simple model calculations listed in Table 1, we suggest that image charges generated in the source and drain electrodes by the charges on the molecule are the most likely origins of this effect. The calculations are carried out using a Hubbard model of the molecule that includes image charges (Fig. 3a, b, Table 1). The results confirm the intuitive physical picture that a charge trapped on the molecule is strongly attracted to its image in the electrode, leading to a localization of the charge close to the electrode. Simple application of Coulomb's law then suggests that the image charge can change the local potential on the benzene ring in contact with the electrode by several eV. The resulting addition energies calculated for $n = \{-1, 0, 1\}$ are in good agreement with the SET experiment for very realistic values of the fitting parameters in the model (see the last footnote in Table 1 for details). These theoretical results are further corroborated by recent spectroscopic studies[21] showing that the LUMO of hexafluorobenzene (C_6F_6) moves by 0.7 eV towards the middle of the HOMO–LUMO gap when this molecule is deposited on a metal surface and ionized through a charge transfer reaction. All together, these findings suggest that the initially injected charges have a localized character on the molecular backbone and can be described as confined polarons. This unorthodox localized charge representation provides a straightforward explanation for the bunching of the molecular charging energies around the neutral state; the energy difference between the bunched states simply represents the rather small energy required to charge both ends of the molecule in two successive steps (Fig. 3c). Further charging of the molecule leads to increased repulsion among the charges, which translates into larger charging energies, as observed experimentally.

We have reported SET data on a single conjugated molecule taken through a series of distinct redox states. Comparison between the intrinsic (redox) addition energies and those measured in the SET reveals a strong perturbation of the molecular properties that we attribute to image charges in the metal electrodes. The results show that the molecule cannot be conceptually separated from the electrodes owing to these electrostatic image charge effects, even when the electronic overlap between the electrodes and the molecule is weak, as evidenced by the observation of single-electron tunnelling phenomena. □

Methods

Total energies from computed ionization potentials

Total energies were calculated at the semiempirical Hartree-Fock Austin Model 1 (AM1) level[22] coupled to a full configuration interaction (CI) scheme within an active space (encompassing five frontier electronic levels) to account for electron correlation effects (see penultimate footnote in Table 1). The wavefunctions have been treated with the restricted open-shell Hartree–Fock (ROHF) formalism for systems with an odd number of electrons. The choice of the AM1 method is driven by its good track record in reproducing the heat of formation of organic molecules. The electrostatic screening of the charges injected into the conjugated backbone by the surrounding medium also has to be taken into account to evaluate properly the total energies of the various redox states. This was achieved in our calculations by using the conductor-like screening model (COSMO)[23] implemented in the Ampac package (Ampac 6-55 ed.; Semichem). The self-consistent reaction field (SCRF) model treats the solvent as an uniform polarizable medium, with a dielectric constant ε, in which the solute is positioned in a suitably shaped cavity. This model is known to provide realistic estimates of molecular total energies in solution when combined to the AM1 parameterization[24].

Addition energies from a Hubbard model

The addition energies of redox states at zero source–drain bias are calculated using the formula $I(n \rightarrow n+1) = E_{\mathrm{tot}}(n+1) + E_{\mathrm{tot}}(n-1) - 2E_{\mathrm{tot}}(n)$, where $E_{\mathrm{tot}}(n)$ is the total energy of molecule with n electrons (see last footnote in Table 1). Included in this energy is the sum of energies of occupied one-electron states as calculated in the Hartree–Fock approximation of the Hubbard model, corrected for double counting of Coulomb repulsion among electrons and the Coulomb energy of the ions experiencing the potential from the mirror charges in the gates. We note that the charge distribution of the molecule in the different redox states are not simple scalings of a fixed charge distribution, as is being assumed in the orthodox capacitance model. Work is in progress (P.H. and K. Flensberg) on giving a full account of the generalization of the capacitance model suggested by the experimental findings of the present work.

Received 23 June; accepted 13 August 2003; doi:10.1038/nature02010.

1. Averin, D. V. & Likharev, K. K. *Mesoscopic phenomena in Solids* (eds Altshuler, B. L., Lee, B. A. & Webb, R. A.) 173–271 (North-Holland, New York, 1991).
2. Kouwenhoven, L. P. *et al.* in *Mesoscopic Electron Transport* (eds Sohn, L. L., Kouwenhoven, L. P. & Schön, G.) 105, Ser. E, Vol. 345 (Klüwer, Dordrecht, 1997).
3. Ralph, D. C., Black, C. T. & Tinkham, M. Gate-voltage studies of discrete electronic states in aluminum nanoparticles. *Phys. Rev. Lett.* **78,** 4087–4090 (1997).
4. Klein, D. L., Roth, R., Lim, A. K. L., Alivisatos, A. P. & McEuen, P. L. A single electron transistor made of a cadmium selenide nanocrystal. *Nature* **389,** 699–701 (1997).
5. Cobden, D. H. *et al.* Transport spectroscopy of single-walled carbon nanotubes. *Physica B*, **249–251,** 132–135 (1998).
6. Tans, S. J., Devoret, M. H., Groeneveld, R. J. A. & Dekker, C. Electron-electron correlations in carbon nanotubes. *Nature* **394,** 761–764 (1998).
7. Park, H. *et al.* Nanomechanical oscillations in a single-C_{60} transistor. *Nature* **407,** 57–60 (2000).
8. Park, J. *et al.* Coulomb blockade and the Kondo effect in single-atom transistors. *Nature* **417,** 722–724 (2002).
9. Liang, W., Shores, M. P., Bockrath, M., Long, J. R. & Park, H. Kondo resonance in a single-molecule transistor. *Nature* **417,** 725–729 (2002).
10. Nygard, J., Cobden, D. H. & Lindelof, P. E. Kondo physics in carbon nanotubes. *Nature* **408,** 342–346 (2000).
11. Zhitenev, N. H., Meng, H. & Bao, Z. Conductance of small molecular junctions. *Phys. Rev. Lett.* **88,** 226801 (2002).
12. Stuhr-Hansen, N., Christensen, J. B., Harrit, N. & Bjørnholm, T. Novel synthesis of protected thiol end-capped stilbenes and oligo(phenylenevinylene)s (OPVs). *J. Org. Chem.* **68,** 1275–1282 (2003).
13. Kubatkin, S. E., Danilov, A. V., Olin, H. & Claeson, T. Tunneling through a single quench-condensed cluster. *J. Low-Temp. Phys.* **118,** 307–316 (2000).
14. Park, H., Lim, A. K. L., Alivisatos, A. P., Park, J. & McEuen, P. L. Fabrication of metallic electrodes with namometer separation by electromigration. *Appl. Phys. Lett.* **75,** 301–303 (1999).
15. van Houten, H., Beenakker, C. W. J. & Staring, A. A. M. in *Single Charge Tunnelling and Coulomb Blockade Phenomena in Nanostructures* Ch. 5 (Plenum, New York, 1992).
16. Likharev, K. K. Single electron devices and their application. *Proc. IEEE* **87,** 606–632 (1999).
17. Danilov, A. V., Golubev, D. S. & Kubatkin, S. E. Tunneling through a multigrain system: Deducing sample topology from nonlinear conductance. *Phys. Rev. B* **65,** 125312–125320 (2002).
18. Kouwenhoven, L. P., Austing, D. G. & Tarucha, S. Few-electron quantum dots. *Rep. Prog. Phys.* **64,** 701–706 (2001).
19. Cobden, D. H. & Nygård, J. Shell filling in closed single-wall carbon nanotube quantum dots. *Phys. Rev. Lett.* **89,** 46803 (2002).
20. Heinze, J., Mortensen, J., Müllen, K. & Schenk, R. The charge storage mechanism of conducting polymers: A voltammetric study on defined soluble oligomers of the phenylene-vinylene type. *J. Chem. Soc. Chem. Commun.* 701–703 (1987).
21. Vondrak, T. & Zhu, X.-Y. Two-photon photoemission study of heterogeneous electron transfer: C_6F_6 on Cu(111). *J. Phys. Chem. B* **103,** 3449–3456 (1999).
22. Dewar, M. J. S., Zoebisch, E. G., Healy, E. F. & Stewart, J. J. P. A new general purpose quantum mechanical molecular model. *J. Am. Chem. Soc.* **107,** 3902–3909 (1985).
23. Klamt, A. & Schürmann, G. J. Cosmo—a new approach to dielectric screening in solvents with explicit expressions for the screening energy and its gradient. *J. Chem. Soc. Perkin Trans. 2* **5,** 799–805 (1993).
24. Pourtois, G., Beljonne, D., Cornil, J., Ratner, M. A. & Brédas, J. L. Photoinduced electron-transfer processes along molecular wires based on phenylenevinylene oligomers: A quantum-chemical insight. *J. Am. Chem. Soc.* **124,** 4436–4447 (2002).
25. Comoretto, D. *et al.* Optical constants of highly stretch-oriented poly(p-phenylene-vinylene): A joint experimental and theoretical study. *Phys. Rev. B* **62,** 10173–10184 (2000).

Acknowledgements We thank K. Flensberg for discussions. Financial support from the European Union under the IST programme 'NANOMOL' (initiated by M. Persson) is acknowledged. Work in Denmark is also supported by the Danish Research Council. The work in Arizona is supported by the Office of Naval Research, National Science Foundation, and the IBM Shared University Research Program. The work in Mons is supported by the Belgian Federal Government 'InterUniversity Attraction Pole in Supramolecular Chemistry and Catalysis' and the Belgian National Fund for Scientific Research. J.C. is a research fellow of the FNRS. A.D. was supported by the Swedish SSF.

Competing interests statement The authors declare that they have no competing financial interests.

Correspondence and requests for materials should be addressed to T.B. (tb@nano.ku.dk).